Journal of Computational Physics 408 (2020) 109280

Contents lists available at ScienceDirect

Journal of Computational Physics

www.elsevier.com/locate/jcp

Unified gas-kinetic wave-particle methods III: Multiscale photon transport

Weiming Li [a], Chang Liu [b], Yajun Zhu [c], Jiwei Zhang [d], Kun Xu [b,e,*]

[a] Laboratory of Computational Physics, Institute of Applied Physics and Computational Mathematics, Beijing 100088, China
[b] Department of Mathematics, Hong Kong University of Science and Technology, Clear Water Bay, Kowloon, Hong Kong, China
[c] National Key Laboratory of Science and Technology on Aerodynamic Design and Research, Northwestern Polytechnical University, Xi'an, Shaanxi 710072, China
[d] Applied and Computational Mathematics Division, Beijing Computational Science Research Center, Beijing 100193, China
[e] HKUST Shenzhen Research Institute, Shenzhen 518057, China

ARTICLE INFO

Article history:
Received 3 April 2019
Received in revised form 21 January 2020
Accepted 22 January 2020
Available online 24 January 2020

Keywords:
Radiative transfer equations
Diffusion equation
Wave-particle formulation
Monte Carlo particle method
Unified gas-kinetic scheme

ABSTRACT

In this paper, we extend the unified gas-kinetic wave-particle (UGKWP) method to multiscale photon transport. In this method, the photon free streaming and scattering processes are treated in an un-splitting way. The photon distribution is described by both discrete simulation particle and analytic distribution function. By accurately recovering the multiscale modeling of the unified gas-kinetic scheme (UGKS), the UGKWP method presents a smooth transition for photon transport from optically thin to optically thick regimes according to the cell's Knudsen number. In the optically thin regime, the UGKWP method performs as a Monte Carlo type particle tracking method, while in the optically thick regime it recovers a diffusion process without particles. The proportion of wave-described and particle-described photons is automatically adapted according to the numerical resolution and local photon scattering physics, i.e., the so-called cell Knudsen number. Compared to the discrete ordinates-based UGKS, the UGKWP method requires less memory and does not suffer from ray effect. Compared to the implicit Monte Carlo (IMC) method, the statistical noise of the UGKWP method is greatly reduced, and the computational efficiency is significantly improved in the optically thick regime. Several numerical examples covering all transport regimes from the optically thin to optically thick ones are computed to validate the accuracy and efficiency of the UGKWP method. In comparison with the UGKS and IMC method, the UGKWP method may have a several-order-of-magnitude reduction in computational cost and memory requirement in solving some multiscale transport problems.

1. Introduction

The radiative transfer equation describes photon propagation in the background medium and has important applications in the fields of astrophysics [1], atmospheric physics [2], and optical imaging [3]. The gray radiative transfer equation with isotropic scattering reads

* Corresponding author at: Department of Mathematics, Hong Kong University of Science and Technology, Clear Water Bay, Kowloon, Hong Kong, China.
E-mail addresses: liweiming@pku.edu.cn (W. Li), cliuaa@connect.ust.hk (C. Liu), zhuyajun@mail.nwpu.edu.cn (Y. Zhu), jwzhang@csrc.ac.cn (J. Zhang), makxu@ust.hk (K. Xu).

https://doi.org/10.1016/j.jcp.2020.109280
0021-9991/

$$\frac{1}{c}\frac{\partial I}{\partial t} + \mathbf{\Omega}\cdot\nabla I = \sigma_s\left(\frac{1}{4\pi}\int_{\mathbb{S}^2} I\,\mathrm{d}\mathbf{\Omega} - I\right) - \sigma_a I + G, \tag{1}$$

where $I(t,\mathbf{x},\mathbf{\Omega})$ is the specific intensity, which is a function of time t, space $\mathbf{x}\in\mathbb{R}^3$, and angle $\mathbf{\Omega}$. In Eq. (1), the speed of light is denoted by c, the scattering coefficient by σ_s, the absorption coefficient by σ_a, and the internal source by G.

There are typically two categories of numerical methods for solving the radiative transfer equations. The first category consists of the deterministic methods with different ways of discretizing and modeling, such as the discrete ordinates method (DOM) [4–7] and the moment methods [8–11]. The second category are the stochastic methods, for example, the Monte Carlo method [12–14]. The Monte Carlo method is a very popular method for solving the radiative transfer problems. In comparison with the deterministic methods, it is more efficient in optically thin regimes, especially for the multidimensional cases, and it does not suffer from the ray effect. However, as a particle method, it unavoidably has statistical noise. In diffusive regimes where the mean free path is small, photons may go through a huge number of scatterings in a macroscopic time scale. Direct simulation of each scattering process for all particles makes the Monte Carlo method very expensive for capturing the diffusive solutions. On the other hand, the diffusion equation could provide good description of the photon transport behavior in the diffusive regime and can be solved very efficiently. Based on this observation, many hybrid methods have been developed in order to improve the overall efficiency in different regimes [15–18], where the Monte Carlo method is used in the optically thin region and the diffusion equation is applied in the optically thick region. However, as far as we know, there is still no unified principle in domain decomposition for capturing different transport regime smoothly.

Another approach towards releasing the stiffness issue in the diffusive regime is to develop asymptotic-preserving (AP) DOM [19–28]. One of the examples is the unified gas-kinetic scheme (UGKS), which couples the particles' transport and collision using a multiscale flux function obtained from the integral solution of the kinetic model equation. The cell size and time step are not restricted by the mean free path and mean collision time. It was developed initially in the field of rarefied gas dynamics [29–31] and has been applied to the fields of radiative transfer [23–28], plasma transport [32], and disperse multi-phase flow [33]. Since it is a discrete ordinate based numerical scheme, it has no statistical noise, but unavoidably suffers from the ray effect in the highly rarefied regime.

The UGKS provides a general methodology to construct multiscale simulation methods for the transport equations [30, 34]. It consists of two governing equations for the microscopic distribution function and macroscopic flow variables on the mesh size and time step scales, and a multiscale evolution solution for the interface distribution function. The time-dependent evolution solution at a cell interface covers the dynamics from the particle free transport to the hydrodynamic wave interaction with the variation of the ratio of the time step to the local particle collision time. The original UGKS is constructed based on the discrete velocity method (DVM) or DOM formulations [29]. However, the corresponding particle version and wave-particle version of UGKS can be constructed as well [35,36]. In this work, we develop a novel unified gas-kinetic wave-particle (UGKWP) method for the multiscale photon transport, which combines the advantages of UGKS and the particle method. To facilitate understanding, a particle-based unified gas-kinetic particle (UGKP) method is described first. In the UGKP method, the photons are described by the particle transport and collision, and this process is controlled by a multiscale integral formulation. More specifically, the Monte Carlo particle model is used to discretize the angular direction of the photon's movement. Based on particles' transport nature in the discretized physical space, particles are categorized into two groups. In a time step, the free-stream particles are accurately tracked by following the trajectories of the simulation particles, while those particles that may get scattered within the time step will be eliminated once scattering happen and then be re-sampled at the beginning of next time step according to the updated macroscopic variables. The fluxes across a cell interface from different type particles are taken into account to update cell averaged macroscopic variables. In such a way, the multiscale process is preserved by coupling particle free streaming and collision. Based on the UGKP method, a more efficient UGKWP method is proposed. Instead of representing all photons by simulation particles, a proportion of photons are represented by an analytical distribution function in the UGKWP method. Therefore, part of the fluxes, which is computed by particles in the UGKP method, could be done analytically with significant reduction in computational cost and statistical noise, especially in the diffusive regime. The multiscale flux function of the UGKS is precisely preserved in the UGKWP implementation. In the diffusive regime, the resulting algorithm would become a standard central difference scheme for the diffusion equation without particles. In the optically thin regime, it gives a particle tracking method same as the Monte Carlo method. In the transition regime, the ratio of the time step over particle collision time determines the transport dynamics, which makes smooth transition between the above two limits. The UGKWP method is not a hybrid method of domain decomposition, but a method with wave-particle duality description in each cell to recover the multiscale modeling in UGKS [30], and high efficiency can be achieved in different regimes.

The rest of this paper is organized as follows. Section 2 briefly recalls the basic idea of the unified gas-kinetic scheme (UGKS) for the linear transport equation. Section 3 presents the UGKP method for linear photon transport. The UGKWP method is described in Section 4, while the extension to radiation-material coupling system is discussed in Section 5. In Section 6, numerical tests are presented to demonstrate the accuracy and efficiency of the UGKWP method. The final section is the conclusion.

2. Review of the UGKS for the linear transport equation

The unified gas-kinetic scheme (UGKS) was initially developed for the problems in the field of rarefied gas dynamics [29,30], and has been successfully applied to radiative transfer problems [23–28] as well. In this section, the simple linear transport equation is used to present the basic idea of the UGKS, based on which the UGKP and UGKWP methods are developed.

Consider the linear transport equation in a purely scattering medium without internal source

$$\frac{1}{c}\frac{\partial I}{\partial t}+\boldsymbol{\Omega}\cdot\nabla I=\sigma\left(\frac{1}{4\pi}\int_{\mathbb{S}^2} I\,\mathrm{d}\boldsymbol{\Omega}-I\right), \tag{2}$$

and the corresponding non-dimensional equation

$$\frac{\epsilon^2}{c}\frac{\partial I}{\partial t}+\epsilon\boldsymbol{\Omega}\cdot\nabla I=\sigma\left(\frac{1}{4\pi}E-I\right), \tag{3}$$

where the non-dimensionalization used is the same as that in [23]. Here $E=\int_{\mathbb{S}^2} I(\boldsymbol{\Omega})\,\mathrm{d}\boldsymbol{\Omega}$, σ denotes the scattering coefficient, and ϵ is the ratio between the typical mean free path and the macroscopic length scale, which is called Knudsen number in gas dynamics.

One important feature of UGKS is the coupled evolution of microscopic distribution and macroscopic quantities. For a finite volume cell m, the discretizations of the two fundamental governing equations for microscopic and macroscopic variables in UGKS are

$$\frac{I_m^{n+1}-I_m^n}{\Delta t}+\sum_{\boldsymbol{\tau}_j\in\partial D_m}\frac{\phi_{\boldsymbol{\tau}_j}}{V_m}=\frac{c\sigma}{\epsilon^2}\left(E_m^{n+1}-I_m^{n+1}\right), \tag{4}$$

and

$$\frac{E_m^{n+1}-E_m^n}{\Delta t}+\sum_{\boldsymbol{\tau}_j\in\partial D_m}\frac{\Phi_{\boldsymbol{\tau}_j}}{V_m}=0, \tag{5}$$

where D_m is the domain covered by the finite volume m, $\boldsymbol{\tau}_j$ represents the interface of the cell boundary ∂D_m, $\mathbf{n}_j$ denotes the outward normal vector of $\boldsymbol{\tau}_j$, and V_m is the volume of cell m. The cell averaged specific intensity I and energy density function E are

$$I_m^n=\frac{1}{V_m}\int_{D_m} I(t^n,\mathbf{x},\boldsymbol{\Omega})\,\mathrm{d}\mathbf{x},$$

and

$$E_m^n=\frac{1}{V_m}\int_{D_m} E(t^n,\mathbf{x})\,\mathrm{d}\mathbf{x},$$

respectively. The microscopic and macroscopic flux terms give

$$\phi_{\boldsymbol{\tau}_j}=\frac{c}{\epsilon\,\Delta t}\int_{t^n}^{t^{n+1}}\int_{\boldsymbol{\tau}_j}\left(\boldsymbol{\Omega}\cdot\mathbf{n}_j\right) I(t,\mathbf{x},\boldsymbol{\Omega})\,\mathrm{d}l\,\mathrm{d}t, \tag{6}$$

and

$$\Phi_{\boldsymbol{\tau}_j}=\int_{\mathbb{S}^2}\phi_{\boldsymbol{\tau}_j}(\boldsymbol{\Omega})\,\mathrm{d}\boldsymbol{\Omega}. \tag{7}$$

Based on the above microscopic and macroscopic governing equations, the key ingredient of the UGKS is the construction of the multiscale flux function by adopting the integral solution of the kinetic model equation (3). Specifically,

$$I(t,\mathbf{x},\boldsymbol{\Omega})=\mathrm{e}^{-\frac{c\sigma(t-t^n)}{\epsilon^2}} I\left(t^n,\mathbf{x}-\frac{c}{\epsilon}\boldsymbol{\Omega}(t-t^n)\right)+\int_{t^n}^{t}\mathrm{e}^{-\frac{c\sigma(t-s)}{\epsilon^2}}\times\frac{c\sigma}{\epsilon^2}\frac{1}{4\pi}E\left(s,\mathbf{x}-\frac{c}{\epsilon}\boldsymbol{\Omega}(t-s)\right)\mathrm{d}s, \tag{8}$$

is used to construct the numerical fluxes in equation (4) and (5). The integral solution couples transport with particle collisions, and bridges the kinetic and the hydrodynamic scale dynamics. Note that the dynamics in the evolution equations of UGKS through equations (4), (5), and (8), is related to time step Δt. The ratio of the local particle collision time and the time step, i.e., the so-called cell's Knudsen number, determines the transport regime of the UGKS.

The numerical flux for the update of microscopic and macroscopic variables is based on the evolution solution from initial piecewise linear reconstructions of I and E. In UGKS, the discretization of I is based on the DOM. It has been proved in [23] that the UGKS provides a free transport solution when σ equals 0, and becomes a standard central difference method for the diffusion equation as ϵ tends to 0 in the diffusion limit. More specifically, in the free transport regime, the governing equation of UGKS for the update of microscopic distribution (4) goes to

$$\frac{I_m^{n+1}-I_m^n}{\Delta t}+\sum_{\boldsymbol{\tau}_j\in\partial D_m}\frac{\phi_{\boldsymbol{\tau}_j}}{V_m}=0, \tag{9}$$

where $\phi_{\boldsymbol{\tau}_j}$ is the UGKS flux in Eq. (6). In the free transport regime, based on a second order reconstruction the flux becomes

$$\begin{aligned}\phi_{\boldsymbol{\tau}_j}=&\lim_{\sigma\to 0}\frac{c}{\epsilon\Delta t}\int_{t^n}^{t^{n+1}}\int_{\boldsymbol{\tau}_j}(\boldsymbol{\Omega}\cdot\mathbf{n}_j)I\left(t^n,\mathbf{x}-\frac{c}{\epsilon}\boldsymbol{\Omega}(t-t^n)\right)\mathrm{d}l\,\mathrm{d}t\\ =&\frac{c}{\epsilon}(\boldsymbol{\Omega}\cdot\mathbf{n}_j)L(\boldsymbol{\tau}_j)\left(\frac{1}{2}[1+\mathrm{sign}(\boldsymbol{\Omega}\cdot\mathbf{n}_j)]I(t^n,\mathbf{x}^l_{\boldsymbol{\tau}_j})+\frac{1}{2}[1-\mathrm{sign}(\boldsymbol{\Omega}\cdot\mathbf{n}_j)]I(t^n,\mathbf{x}^r_{\boldsymbol{\tau}_j})\right)\\ &-\frac{c^2\Delta tL(\boldsymbol{\tau}_j)}{2\epsilon^2}(\boldsymbol{\Omega}\cdot\mathbf{n}_j)\left(\frac{1}{2}[1+\mathrm{sign}(\boldsymbol{\Omega}\cdot\mathbf{n}_j)]\left(\boldsymbol{\Omega}\cdot\nabla_{\mathbf{x}}I(t^n,\mathbf{x}^l_{\boldsymbol{\tau}_j})\right)\right.\\ &\left.+\frac{1}{2}[1-\mathrm{sign}(\boldsymbol{\Omega}\cdot\mathbf{n}_j)]\left(\boldsymbol{\Omega}\cdot\nabla_{\mathbf{x}}I(t^n,\mathbf{x}^r_{\boldsymbol{\tau}_j})\right)\right),\end{aligned} \tag{10}$$

where $L(\boldsymbol{\tau}_j)$ is the length of the cell interface $\boldsymbol{\tau}_j$ with outward unit vector $\mathbf{n}_j$, $I(t^n,\mathbf{x}^l_{\boldsymbol{\tau}_j})$, $\nabla_{\mathbf{x}}I(t^n,\mathbf{x}^l_{\boldsymbol{\tau}_j})$ are point-wise value and gradient of I at the left hand side of the interface, and $I(t^n,\mathbf{x}^r_{\boldsymbol{\tau}_j})$, $\nabla_{\mathbf{x}}I(t^n,\mathbf{x}^r_{\boldsymbol{\tau}_j})$ are on the right hand side of the interface. When first order approximation is used in the initial reconstruction, the expression of $\phi_{\boldsymbol{\tau}_j}$ could be further simplified to

$$\phi_{\boldsymbol{\tau}_j}=\frac{c}{\epsilon}(\boldsymbol{\Omega}\cdot\mathbf{n}_j)L(\boldsymbol{\tau}_j)\left(\frac{1}{2}[1+\mathrm{sign}(\boldsymbol{\Omega}\cdot\mathbf{n}_j)]I_m^n+\frac{1}{2}[1-\mathrm{sign}(\boldsymbol{\Omega}\cdot\mathbf{n}_j)]I_k^n\right), \tag{11}$$

where k is the index for neighboring cell of the cell m with the interface $\boldsymbol{\tau}_j$ between them. In the diffusive limit, the UGKS becomes

$$\frac{E_m^{n+1}-E_m^n}{\Delta t}+\sum_{\boldsymbol{\tau}_j\in\partial D_m}\frac{\Phi_{\boldsymbol{\tau}_j}}{V_m}=0,\quad \Phi_{\boldsymbol{\tau}_j}=-\frac{c}{3\sigma}L(\boldsymbol{\tau}_j)\mathbf{n}_j\cdot\left(\frac{E_k^n-E_m^n}{|\mathbf{x}_k-\mathbf{x}_m|}\mathbf{n}_{mk}\right), \tag{12}$$

where $\mathbf{x}_k$ and $\mathbf{x}_m$ are the barycenters of cell k and m with the unit vector $\mathbf{n}_{mk}$ from $\mathbf{x}_m$ to $\mathbf{x}_k$.

More details on the asymptotic analysis of the UGKS for the radiative transfer equation can be found in [23] and [24].

3. The unified gas-kinetic particle (UGKP) method

In this section, we present a unified gas-kinetic particle (UGKP) method. Following the direct modeling methodology of UGKS, the evolution of microscopic simulation particle is coupled with the evolution of macroscopic energy in the UGKP method. In the following, the scheme for the evolution of microscopic particles and macroscopic energy field will be introduced. For simplicity, the method will be presented for the two-dimensional case on uniform Cartesian mesh. Its extension to non-uniform mesh and 3D is straightforward.

3.1. Multiscale particle evolution

The evolution of the simulation particle follows the integral solution of the linear transport equation (3),

$$I(t,\mathbf{x},\boldsymbol{\Omega})=\int_0^t e^{-\frac{c\sigma}{\epsilon^2}(t-s)}\frac{c\sigma}{\epsilon^2}\frac{1}{4\pi}E\left(s,\mathbf{x}-\frac{c}{\epsilon}\boldsymbol{\Omega}(t-s),\boldsymbol{\Omega}\right)ds+e^{-\frac{c\sigma}{\epsilon^2}t}I_0\left(\mathbf{x}-\frac{c}{\epsilon}\boldsymbol{\Omega}t\right). \tag{13}$$

For a second order accuracy, the local equilibrium E is expanded in space and time,

$$E\left(s,\mathbf{x}-\frac{c}{\epsilon}\boldsymbol{\Omega}(t-s),\boldsymbol{\Omega}\right)\approx E(t,\mathbf{x},\boldsymbol{\Omega})+E_{\mathbf{x}}(t,\mathbf{x},\boldsymbol{\Omega})\frac{c}{\epsilon}\boldsymbol{\Omega}(s-t)+E_t(t,\mathbf{x},\boldsymbol{\Omega})(s-t), \tag{14}$$

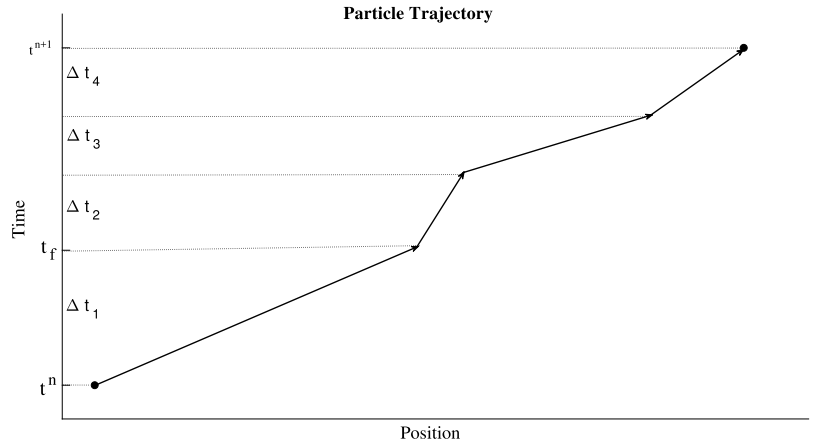

Fig. 1. Particle trajectory in Monte Carlo method for $t^n < t \le t^{n+1}$ with sub time steps Δt_1, Δt_2, Δt_3 and Δt_4.

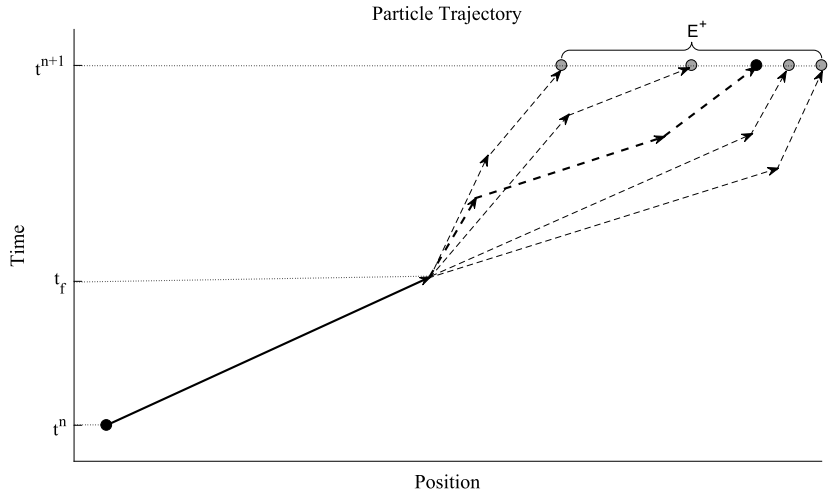

Fig. 2. UGKP's treatment of particle evolution for $t^n < t \le t^{n+1}$.

the evolution solution becomes

$$I(t,\mathbf{x},\mathbf{\Omega}) = \left(1-e^{-\frac{c\sigma}{\epsilon^2}t}\right)\frac{1}{4\pi}E^+(t,\mathbf{x},\mathbf{\Omega}) + e^{-\frac{c\sigma}{\epsilon^2}t}I_0(\mathbf{x}-\frac{c}{\epsilon}\mathbf{\Omega}t), \tag{15}$$

where

$$E^+(t,\mathbf{x},\mathbf{\Omega}) = E(t,\mathbf{x},\mathbf{\Omega}) + \frac{e^{-\frac{c\sigma}{\epsilon^2}t}\left(t+\frac{\epsilon^2}{c\sigma}\right)-\frac{c\sigma}{\epsilon^2}}{1-e^{-\frac{c\sigma}{\epsilon^2}t}}\left(E_t(\mathbf{\Omega})+\frac{c}{\epsilon}\Omega E_{\mathbf{x}}(\mathbf{\Omega})\right), \tag{16}$$

and the first order approximation gives

$$E^+(t,\mathbf{x},\mathbf{\Omega}) = E(t,\mathbf{x},\mathbf{\Omega}). \tag{17}$$

The integral solution (15) presents a multiscale evolution, which is used for the particle transport in UGKP method. The above solution implies that the simulation particle has a probability of $\exp(-\frac{c\sigma}{\epsilon^2}t)$ to free stream and has a probability of $1-\exp(-\frac{c\sigma}{\epsilon^2}t)$ to get scattered. The scattering particle follows a velocity distribution $E^+(t,x,\mathbf{\Omega})$. For the sake of simplicity, the first order approximation Eq. (17) is used in this paper, and it has been proved in [35] that the multiscale property will still be preserved. Different from the traditional Monte Carlo method which tracks the trajectory of each particle as shown in Fig. 1, the UGKP method tracks particle trajectory until it gets scattered. The scattering particles will get re-sampled from their distribution Eq. (17) once their total energy is obtained at the end of time step, as shown in Fig. 2. The free-streaming particles are named as the E_f particles, and the scattering particles are named as the E^+ particles. The total energy of the E^+ particles is called E^+ energy. In the UGKP method, we do not need to use a small time step to resolve each scattering

process. Multiple scattering can happen for each particle within a time step. Therefore, the UGKP achieves a high efficiency compared to the traditional Monte Carlo method.

The free stream time t_f is defined as the time at the first scattering for each particle. According to Eq. (15), the time t_f can be obtained for each particle as

$$t_f = -\frac{\epsilon^2}{c\sigma}\ln\xi, \tag{18}$$

where ξ is a random number which follows a uniform distribution on $(0,1)$. For the current scheme, the free stream time t_f for each particle within the cell is generated according to the opacity of the cell at the beginning of the time step. Simulation particles can be categorized into two groups based on t_f. The first group of simulation particle satisfies

$$t_f \geq \Delta t \tag{19}$$

and does not suffer any collision during a time step $\Delta t = t^{n+1} - t^n$. The particle position for the collisionless particle is updated by

$$\mathbf{x}^{n+1} = \mathbf{x}^n + \frac{c\boldsymbol{\Omega}^n}{\epsilon}\Delta t. \tag{20}$$

The second group of particle satisfies $t_f < \Delta t$, and those particles may suffer one or multiple times of collision during $[t_f, t^{n+1}]$. In UGKP, these particles are tracked for $t \in [t^n, t_f)$ and get re-sampled from $E^+(t^{n+1}, \mathbf{x}, \boldsymbol{\Omega})$ at t^{n+1} at the beginning of next time step. The energy $E^+(t^{n+1}, \mathbf{x}, \boldsymbol{\Omega})$ is obtained from the evolved macroscopic energy. Therefore, particles will be tracked to the end of the time step $t = \Delta t$ if $t_f \geq \Delta t$, or up to the time $t = t_f$ if $t_f < \Delta t$. It is worth noticing that at a cell interface with a large variation of opacity of neighboring cells, different t_f will be generated for these particles across the interface. For example, for a particle within cell m, the free motion time generated according to the current cell's opacity is $\min(t_f, \Delta t)$. If the particle goes through the cell interface at $t = t_b$ and moves into the neighboring cell m^*, another free motion time according to the opacity of cell m^* will be used for the particle tracking process in cell m^*, i.e., $t' = \min(t_f^*, \Delta t - t_b)$. In such a way, the particle transport process between zones with large-opacity-variation can be well resolved. In UGKP method, the evolution of particle and macroscopic energy are closely coupled. The multiscale evolution equation of macroscopic energy is given next.

3.2. Multiscale macroscopic energy evolution

In a finite volume framework, the update of the macroscopic variable follows

$$E_m^{n+1} = E_m^n - \frac{\Delta t}{V_m}\sum_{\boldsymbol{\tau}_j \in \partial D_m}\Phi_{E,\boldsymbol{\tau}_j} - \frac{1}{V_m}\sum_{\boldsymbol{\tau}_j \in \partial D_m} W_{\boldsymbol{\tau}_j}, \tag{21}$$

where the flux Φ_E is the diffusive flux and W is the contribution of the free streaming flux. Based on Eq. (13), the diffusive flux is computed same as that in the UGKS,

$$\Phi_{E,\boldsymbol{\tau}_j} = \frac{c}{\epsilon\Delta t}\int_{t^n}^{t^{n+1}}\int_{t^n}^{t}\int_{\boldsymbol{\tau}_j}\int_{\mathbb{S}^2}\left(\boldsymbol{\Omega}\cdot\mathbf{n}_j\right)\frac{c\sigma_{\boldsymbol{\tau}_j}}{\epsilon^2}\mathrm{e}^{-\frac{c\sigma_{\boldsymbol{\tau}_j}(t-s)}{\epsilon^2}}\frac{1}{4\pi}E\left(s, \mathbf{x} - \frac{c}{\epsilon}(t-s)\boldsymbol{\Omega}\right)\mathrm{d}\boldsymbol{\Omega}\,\mathrm{d}l\,\mathrm{d}s\,\mathrm{d}t. \tag{22}$$

With a piecewise linear reconstruction for E,

$$E\left(s, \mathbf{x}_{\boldsymbol{\tau}_j} - \frac{c}{\epsilon}(t-s)\boldsymbol{\Omega}\right) = E(t^n, \mathbf{x}_{\boldsymbol{\tau}_j}) + \left.\frac{\partial E}{\partial t}\right|_{(t^n, \mathbf{x}_{\boldsymbol{\tau}_j})}(s - t_n) - \frac{c}{\epsilon}(t-s)\boldsymbol{\Omega}\cdot\nabla E|_{(t^n, \mathbf{x}_{\boldsymbol{\tau}_j})}, \tag{23}$$

and the explicit central difference discretization of ∇E,

$$\nabla E(t^n, \mathbf{x}_{\boldsymbol{\tau}_j}) \approx \frac{E_m^n - E_k^n}{|\mathbf{x}_m - \mathbf{x}_k|}\mathbf{n}_{km}, \tag{24}$$

where $\mathbf{x}_m$, $\mathbf{x}_k$ are the barycenters of cells m and k with the same interface $\boldsymbol{\tau}_j$. With the length $L(\boldsymbol{\tau}_j)$ of $\boldsymbol{\tau}_j$, the diffusive flux is given by

$$\Phi_{E,\boldsymbol{\tau}_j} = L(\boldsymbol{\tau}_j)\alpha_{\boldsymbol{\tau}_j}\mathbf{n}_j\cdot\left(\frac{E_m^n - E_k^n}{|\mathbf{x}_m - \mathbf{x}_k|}\mathbf{n}_{km}\right), \tag{25}$$

where

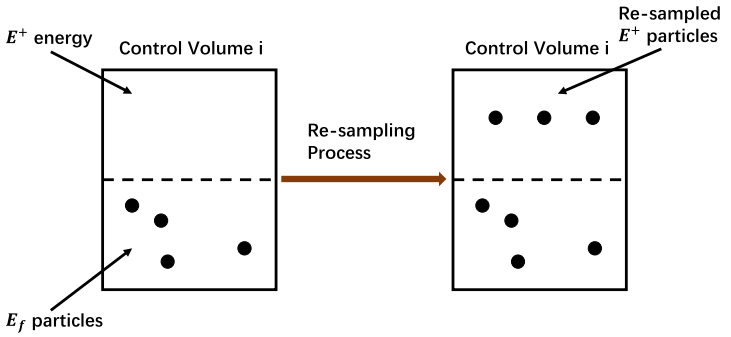

Fig. 3. UGKP composition of particles and re-sampling particles in a cell i at $t = t^{n+1}$. The left figure illustrates the updated solutions of macroscopic variables and microscopic particles at the end of each time step, and the right figure is the update of microscopic particles at the beginning of next time step.

$$\alpha_{\boldsymbol{\tau}_j} = -\frac{c}{3\sigma_{\boldsymbol{\tau}_j}}\left(-\frac{2}{\left(\frac{c\sigma_{\boldsymbol{\tau}_j}\Delta t}{\epsilon^2}\right)}\left(1-\mathrm{e}^{-\frac{c\sigma_{\boldsymbol{\tau}_j}\Delta t}{\epsilon^2}}\right)+\left(1+\mathrm{e}^{-\frac{c\sigma_{\boldsymbol{\tau}_j}\Delta t}{\epsilon^2}}\right)\right). \tag{26}$$

The free transport flux W is from the free streaming particles across the cell interface, which is computed by

$$W_{\boldsymbol{\tau}_j} = \sum_{k\in S(\boldsymbol{\tau}_j)} \mathrm{sign}(\mathbf{n}_j\cdot\boldsymbol{\Omega}_k)\omega_k, \tag{27}$$

where ω_k and $\boldsymbol{\Omega}_k$ are respectively the weight and velocity of the particle k, and $S(\boldsymbol{\tau}_j)$ is the set of all particles moving across interface $\boldsymbol{\tau}_j$ during the free streaming process. The above free streaming flux recovers the free transport part of UGKS flux in Eq. (13),

$$\Phi_{f,\boldsymbol{\tau}_j} = \frac{c}{\epsilon\Delta t}\int_{t^n}^{t^{n+1}}\int_{\boldsymbol{\tau}_j}\int_{\mathbb{S}^2}\left(\boldsymbol{\Omega}\cdot\mathbf{n}_j\right)\mathrm{e}^{-\frac{c\sigma_{\boldsymbol{\tau}_j}(t-t^n)}{\epsilon^2}} I_0\left(t^n,\mathbf{x}-\frac{c}{\epsilon}(t-t^n)\boldsymbol{\Omega},\boldsymbol{\Omega}\right)\mathrm{d}\boldsymbol{\Omega}\,\mathrm{d}l\,\mathrm{d}t. \tag{28}$$

With the diffusive flux Eq. (25) and the free transport flux Eq. (27), the macroscopic energy E^{n+1} can be updated by

$$E_m^{n+1} = E_m^n - \frac{\Delta t}{V_m}\sum_{\boldsymbol{\tau}_j\in\partial D_m} L(\boldsymbol{\tau}_j)\alpha_{\boldsymbol{\tau}_j}\mathbf{n}_j\cdot\left(\frac{E_m^n-E_k^n}{|\mathbf{x}_m-\mathbf{x}_k|}\mathbf{n}_{km}\right) - \frac{1}{V_m}\sum_{\boldsymbol{\tau}_j\in\partial D_m} W_{\boldsymbol{\tau}_j}. \tag{29}$$

With the updated E^{n+1}, the energy E^+ of the scattering particles can be obtained and be used to re-generate these particles at the beginning of next time step,

$$E_m^+ = E_m^{n+1} - \frac{1}{V_m}\sum_{k\in Q(m)}\omega_k, \tag{30}$$

where $Q(m)$ is the set of E_f particles remaining in cell m at t^{n+1}. In summary, the UGKP evolves the particle and macroscopic variable within a time step. Based on the update of total energy and the energy of remaining particle inside each cell, the energy E^+ for the scattering particles can be obtained and used to re-sample new particles at the beginning of next time step, see Fig. 3. The evolution of microscopic and macroscopic quantities are closely coupled, and the algorithm of the UGKP method is shown in Fig. 4.

4. Unified gas-kinetic wave-particle (UGKWP) method

4.1. The multiscale evolution of particle and macroscopic variable

In the UGKP method, the particles of E^+ are re-sampled from an equilibrium distribution at $t = t^{n+1}$. For determining the weights of the particles, a reference weight, w^*, is specified. In cell m, the number of re-sampled E^+ particles are

$$N_m = \begin{cases} 0, & \text{if } E^+V_m < w^*, \\ \lceil \frac{E^+V_m}{w^*} \rceil, & \text{if } E^+V_m \geq w^*, \end{cases} \tag{31}$$

where V_m is the volume of cell m. If $N_m > 0$, the re-sampled particle weight is assigned to be $\frac{E^+V_m}{N_m}$ which is close to the reference weight w^*, and the weights of all sampled particles in cell m are added up to E^+V_m. The energy E^+

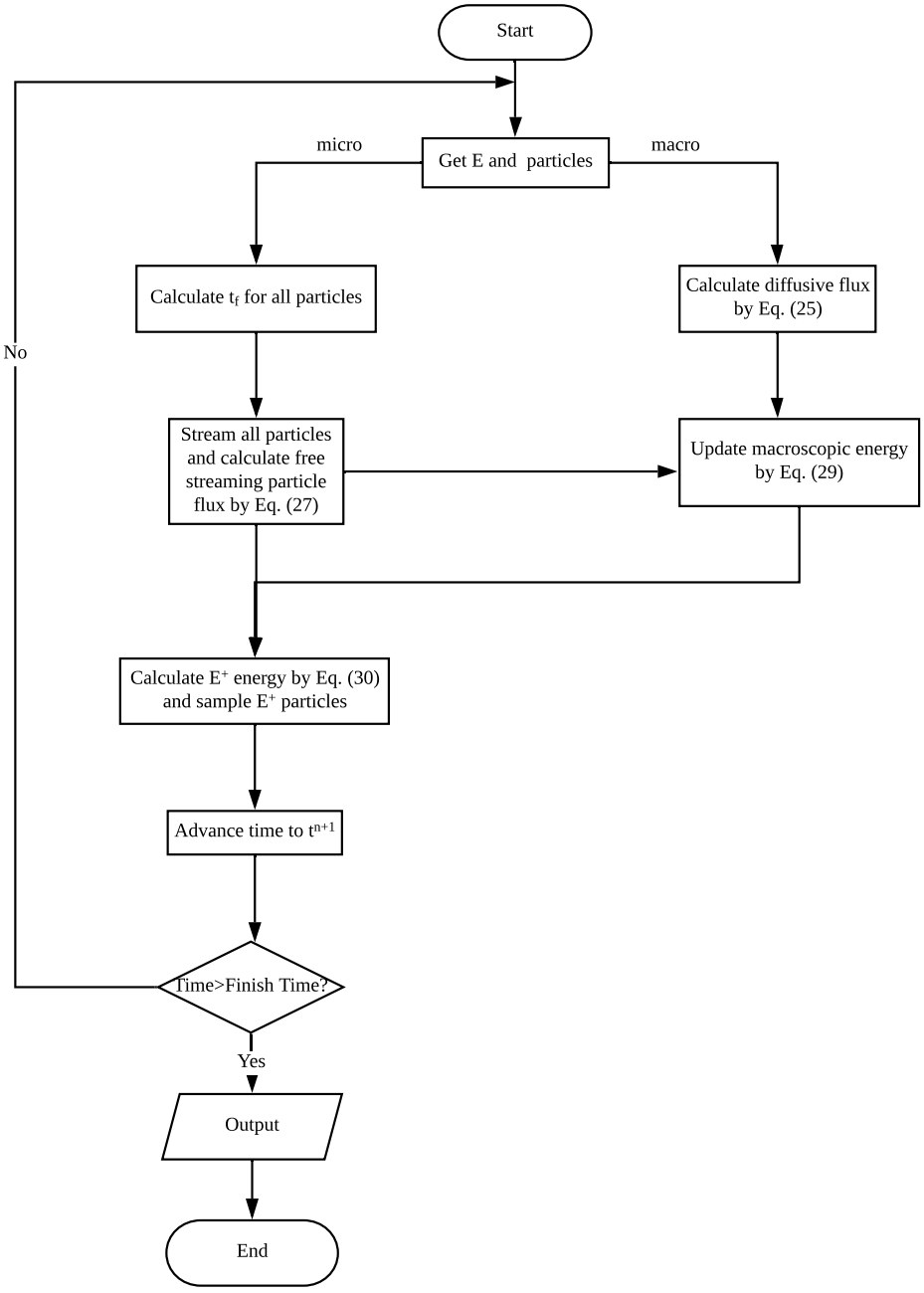

Fig. 4. Flowchart of UGKP method.

is linearly interpolated within each control volume, and the acceptance-rejection method is used to sample the particle position according to the reconstructed energy E^+.

According to the integral solution (13), all re-sampled E^+ particles have a probability $1-\mathrm{e}^{-\frac{c\sigma\Delta t}{\epsilon^2}}$ to get scattered in the next time step from t^{n+1} to t^{n+2}. The scattering E^+ particles in $t\in[t^{n+1},t^{n+2}]$ are denoted as E_W^+ particles and the non-scattering E^+ particles as E_P^+ particles. For the E_W^+ particles, they will get scattered in the next time step. According to the UGKS formulation, these scattering particles can be represented by an analytical distribution function. Their contribution to the free transport flux can be computed analytically. By making use of this property, the unified gas-kinetic wave-particle (UGKWP) method is proposed. In the UGKWP method, only the E_P^+ particles need to be re-sampled. As shown in [35], the positions of E_P^+ particles can be simply sampled from a piecewise constant reconstruction of the E_P^+ energy, which will not affect the multiscale property of UGKWP method. These particles will keep free transport in the time $t\in[t^{n+1},t^{n+2}]$. The UGKWP method improves UGKP in two aspects:

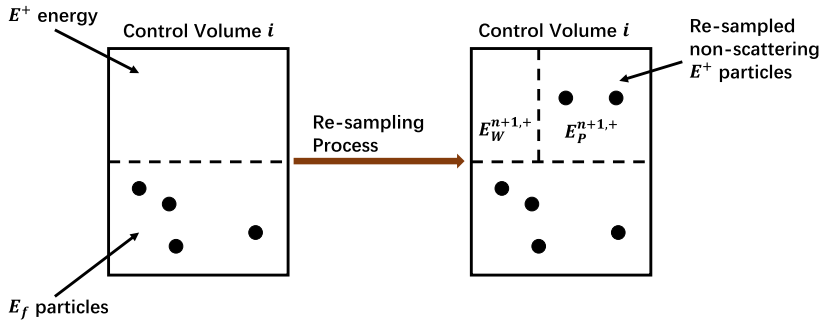

Fig. 5. UGKWP composition of particles and the re-sampling process in a control volume cell i at $t = t^{n+1}$. The left figure illustrates the updated solutions of macroscopic variables and microscopic particles at the end of each time step, and the right figure is the update of microscopic particles and un-sampled particles of $E_W^{n+1,+}$ at the beginning of next time step.

1. Only E_P^+ particles are sampled as shown in Fig. 5.
2. The free transport flux contributed by E_W^+ can be calculated analytically.

The finite volume energy evolution follows

$$E_m^{n+1} = E_m^n - \frac{\Delta t}{V_m} \sum_{\boldsymbol{\tau}_j \in \partial D_m} (\Phi_{E,\tau_j} + \Phi_{fw,\boldsymbol{\tau}_j}) - \frac{1}{V_m} \sum_{\boldsymbol{\tau}_j \in \partial D_m} W_{\boldsymbol{\tau}_j}, \tag{32}$$

where the diffusive flux $\Phi_{E,\boldsymbol{\tau}_j}$ is computed using Eq. (25), and the free transport flux contributed by E_W^+ is calculated by

$$\begin{aligned} \Phi_{fw,\boldsymbol{\tau}_j} =& \frac{c}{\epsilon \Delta t} \int_{t^n}^{t^{n+1}} \int_{\boldsymbol{\tau}_j} \int_{\mathcal{S}^2} (\Omega \cdot \mathbf{n}_j) e^{-\frac{c\sigma \boldsymbol{\tau}_j (t-t^n)}{\epsilon^2}} E^+ \left(t^n, x - \frac{c}{\epsilon} \left(t - t^n \right) \boldsymbol{\Omega}, \boldsymbol{\Omega} \right) d\boldsymbol{\Omega} dl dt \\ & - \frac{c}{\epsilon \Delta t} \int_{t^n}^{t^{n+1}} \int_{\boldsymbol{\tau}_j} \int_{\mathcal{S}^2} (\boldsymbol{\Omega} \cdot \mathbf{n}_j) E_P^+ \left(t^n, x - \frac{c}{\epsilon} \left(t - t^n \right) \boldsymbol{\Omega}, \boldsymbol{\Omega} \right) d\boldsymbol{\Omega} dl dt. \end{aligned} \tag{33}$$

The free transport flux $W_{\boldsymbol{\tau}_j}$ contributed from the particles in Eq. (32) is computed by particle tracking,

$$W_{\boldsymbol{\tau}_j} = \sum_{k \in S(\boldsymbol{\tau}_j)} \text{sign}(\mathbf{n}_j \cdot \boldsymbol{\Omega}_k) \omega_k, \tag{34}$$

where $S(\boldsymbol{\tau}_j)$ is the set of all particles which are transported across the cell interface $\boldsymbol{\tau}_j$ during the free streaming process. In the particle free transport process, the re-sampled E_P^+ particles will always have $t_f > \Delta t$ and keep free transport without collision in the whole time step. The other particles from E_f will transport according to their individually generated t_f. With the solution of E^{n+1}, Eq. (30) is used to get E^+, which is then divided into

$$E_P^+ = \mathrm{e}^{-\frac{c\sigma \Delta t}{\epsilon^2}} E^+, \tag{35}$$

and

$$E_W^+ = E^+ - E_P^+, \tag{36}$$

and only particles from E_P^+ will be generated and keep on free transport in next time step. The algorithm of the UGKWP method is shown in Fig. 6.

4.2. Properties of UGKWP algorithm

The unified gas-kinetic wave-particle method satisfies the following properties:

1. The microscopic and macroscopic evolutions are consistently evaluated based on the wave-particle decomposition. The updated macroscopic energy density E is the sum of the energy from the un-scattering particles E_f and the scattering ones $E^+ = E_P^+ + E_W^+$. The evolution of E_W^+ particles can be evaluated analytically.

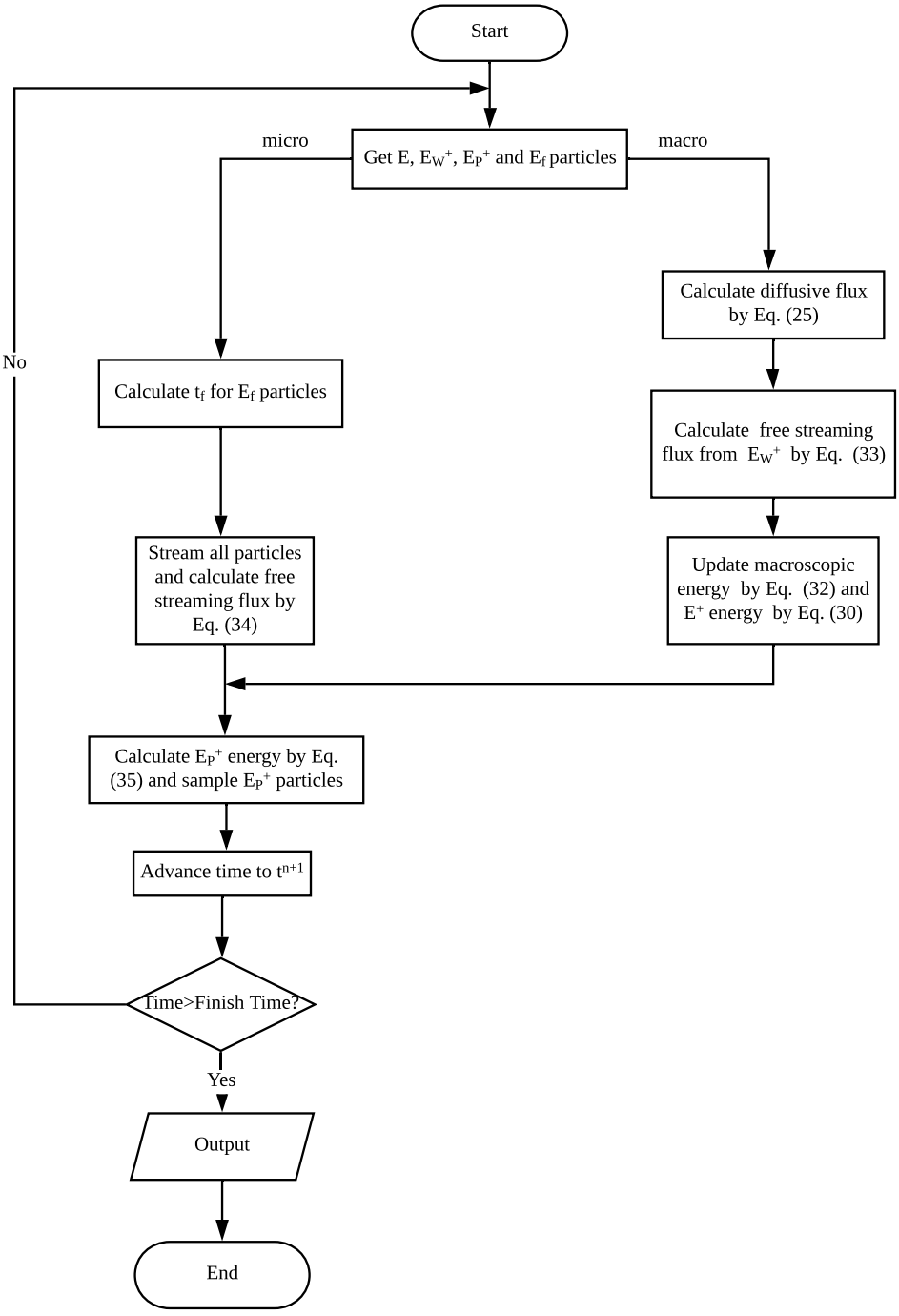

Fig. 6. Flowchart of UGKWP method.

2. In the diffusive limit, $\epsilon \to 0$ and $\exp(-\frac{\sigma_{\tau_j}\Delta t}{\epsilon^2}) \to 0$, essentially no particle can be freely transported and survived within a time step. Therefore, no particle is re-sampled from the E^+ energy. The algorithm becomes a time-explicit central difference solver of the diffusion equation. For instance, in 1D case with uniform grid, the scheme tends to the following limiting equation

$$\frac{E_j^{n+1}-E_j^n}{\Delta t}-\frac{1}{\Delta x}\left(\frac{c}{3\sigma_{j+\frac{1}{2}}}\frac{E_{j+1}^n-E_j^n}{\Delta x}-\frac{c}{3\sigma_{j-\frac{1}{2}}}\frac{E_j^n-E_{j-1}^n}{\Delta x}\right)=0. \tag{37}$$

Note that in the diffusion regime, different from DOM there is no velocity space discretization in UGKWP method. The UGKWP will become a solver for the macroscopic variable only and the scheme becomes very efficient.

3. In the free transport limit, $\sigma \to 0$ and $\exp(-\frac{\sigma_{\tau_j}\Delta t}{\epsilon^2}) \to 1$, each particle is traced exactly by free transport with probability 1. In this case, the UGKWP method would recover the exact solution of individual particles, which is the same as a purely particle method.

5. UGKWP for gray radiative transfer and material energy evolution system

This section extends UGKWP method to solve the coupled system of gray radiative transfer and material temperature equation. For the radiation passing through a material with constant specific heat capacity, the coupled system is

$$\begin{cases} \dfrac{\epsilon^2}{c}\dfrac{\partial I}{\partial t} + \epsilon \boldsymbol{\Omega}\cdot\nabla I = \sigma\left(\dfrac{1}{4\pi}acT^4 - I\right) + G, \\ \epsilon^2 C_v \dfrac{\partial T}{\partial t} = \sigma\left(\displaystyle\int_{\mathbb{S}^2} I(\boldsymbol{\Omega})\,\mathrm{d}\boldsymbol{\Omega} - acT^4\right). \end{cases} \tag{38}$$

Define $u_m = C_v T$, $u_r = aT^4$ and $\beta = u_r/u_m$, the second equation can be written as

$$\frac{\partial u_r}{\partial t} = \beta\frac{\sigma}{\epsilon^2}\left(\int_{\mathbb{S}^2} I(\boldsymbol{\Omega})\,\mathrm{d}\boldsymbol{\Omega} - cu_r\right). \tag{39}$$

The implicit Monte Carlo method proposed by Fleck and Cummings introduces an effective scattering process [12], which approximates the absorption and emission of radiation by background medium. This treatment allows it to take larger time step than that used in a purely explicit method. It has been shown to be an effective approach for solving time-dependent, non-linear, radiative transfer problems, and is widely used in the radiative transfer community. Here the same semi-implicit discretization for material temperature evolution will be employed. Specifically, Eq. (39) is discretized by

$$\frac{u_r^{n+1} - u_r^n}{\Delta t} = \beta^n\frac{\sigma}{\epsilon^2}\left(E - cu_r^{n+1}\right), \tag{40}$$

which gives

$$u_r^{n+1} = \frac{1}{1 + c\beta^n \times \frac{\sigma\Delta t}{\epsilon^2}}u_r^n + \frac{\beta^n \times \frac{\sigma\Delta t}{\epsilon^2}}{1 + c\beta^n \times \frac{\sigma\Delta t}{\epsilon^2}}E. \tag{41}$$

With the definition

$$\sigma_a = \frac{\sigma}{1 + c\beta^n \times \frac{\sigma\Delta t}{\epsilon^2}}, \quad \sigma_s = \sigma - \sigma_a, \tag{42}$$

substituting Eq. (41) into Eq. (38) yields

$$\frac{\epsilon^2}{c}\frac{\partial I}{\partial t} + \epsilon\boldsymbol{\Omega}\cdot\nabla I = \sigma_s\left(\frac{1}{4\pi}E - I\right) + \sigma_a\left(\frac{1}{4\pi}cu_r^n - I\right) + G. \tag{43}$$

An operator splitting approach is used to solve the above equation subsequently by the linear kinetic equation

$$\frac{\epsilon^2}{c}\frac{\partial I}{\partial t} + \epsilon\boldsymbol{\Omega}\cdot\nabla I = \sigma_s\left(\frac{1}{4\pi}E - I\right) + G, \tag{44}$$

the energy exchange,

$$\frac{\epsilon^2}{c}\frac{\partial I}{\partial t} = \sigma_a\left(\frac{1}{4\pi}cu_r^n - I\right), \tag{45}$$

and the update of material energy. Here Eq. (44) is solved using the algorithm introduced in Section 4. The exact solution of Eq. (45) is

$$I^{n+1} = \exp\left(-\frac{c\sigma_a\Delta t}{\epsilon^2}\right)I^* + \left[1 - \exp\left(-\frac{c\sigma_a\Delta t}{\epsilon^2}\right)\right]\frac{1}{4\pi}cu_r^n, \tag{46}$$

where I^* is solved from Eq. (44) by the UGKWP method. The exponential decay term in Eq. (46) is implemented by modifying the weight of particles, while the source term in Eq. (46) is added to E^+ energy. Afterwards, the energy change of particles is summed up, and the material temperature and u_r are updated by energy conservation. The above UGKWP can be further improved if the technique in [25] is incorporated into the current scheme, where both macroscopic equations for the radiation energy and material energy are solved iteratively first before updating the radiation intensity I.

6. Numerical experiments

In this section, we present six numerical examples to validate the proposed UGKWP method. In all these examples, the results of the UGKWP method are compared with our implementation of a Monte Carlo method. In the Monte Carlo method, for the purely scattering medium, particles are accurately tracked during each scattering process. For the cases of radiation-material coupling, the same semi-implicit time discretization as the IMC method in Eq. (40)-(41), and the same operator splitting strategy as the UGKWP method in Eq. (44)-(45), are employed. The effective scattering part is solved by accurately tracking each scattering process, while Eq. (45) is implemented for decreasing the particle energy by an exponential factor, and re-sampling particles are coming from a piecewise constant spatial reconstruction of the source term.

In all examples, the UGKWP results are in good agreement with that of the Monte Carlo method. At the same time, the UGKWP method is more efficient and less noisy compared with the Monte Carlo method in the near diffusive regime. All computations are performed for a sequential code on a computer with Intel i7-8700K CPU and 64 GB memory. In all simulations, the time step is determined by $\Delta t = \text{CFL}\epsilon\Delta x/c$, with $\text{CFL} = 0.4$ for 1D examples and $\text{CFL} = 0.2$ for 2D examples.

6.1. Inflow into purely scattering homogeneous medium

We first consider the behavior of UGKWP method for purely scattering process in homogeneous medium. Tests in this section are for the non-dimensional linear equation

$$\epsilon\frac{\partial I}{\partial t}+\mu\frac{\partial I}{\partial x}=\frac{\sigma}{\epsilon}\left(\frac{1}{2}E-I\right),$$

with $\sigma = 1$, defined on the semi-infinite spatial domain $x \in [0, \infty)$ with an isotropic inflow condition imposed on the left boundary. For the numerical simulation, the spatial domain is taken to be $[0, 1]$. Inflow boundary condition is imposed at $x = 0$ with the incoming specific intensity $I(t, 0, \mu) = \frac{1}{2}$. The initial value is $I(\mu) = 0$ for all x.

The results of both UGKWP method and the Monte Carlo method are obtained using 200 cells in space. Since we are targeting to develop a method that automatically bridges the optically thin and optically thick regimes, the parameters in the tests cover the rarefied ($\epsilon \gg \Delta x$), the intermediate ($\epsilon \approx \Delta x$), and the diffusive ($\epsilon \ll \Delta x$) regimes, as defined in [37]. When ϵ is small, i.e. in the diffusive regime, the current method can use a much larger cell size and time step than the particle mean free path and collision time. Also, due to the exponential factor in re-sampling, fewer particles are used in the UGKWP method than that of the Monte Carlo method when ϵ is small, and the UGKWP method becomes much more efficient and less noisy than the Monte Carlo method in this case. Table 1 compares the computational time of the Monte Carlo method and the UGKWP method for different ϵ, while Table 2 compares the maximum number of particles used. Notice that no particle is generated in UGKWP method when $\epsilon = 10^{-4}$ and the method becomes a diffusion equation solver automatically. For $\epsilon = 10^{-4}$, the Monte Carlo method takes more than half an hour while the UGKWP method takes only 16 seconds. It shows that the UGKWP method is much more efficient than the Monte Carlo method in the diffusive regime.

In Fig. 7 the numerical results of UGKWP method are compared with the solutions of the Monte Carlo method for different ϵ. In this example, the UGKWP method gives solutions which are almost identical with the Monte Carlo solution in all flow regimes. Also, note that the UGKWP solution is smooth for $\epsilon = 10^{-4}$, while the Monte Carlo solution has statistical noise.

6.2. Inflow into purely scattering heterogeneous medium

We next consider the UGKWP method for purely scattering heterogeneous medium. For this example, the set-up for the computational domain as well as that of the initial and boundary conditions are the same as that in the previous case. Tests in this section are for the dimensional linear equation

$$\frac{\partial I}{\partial t}+\mu\frac{\partial I}{\partial x}=\sigma\left(\frac{1}{2}E-I\right).$$

Both the UGKWP method and the Monte Carlo method use 200 cells in space.

We calculate two test cases. For the first test case, $\sigma = 10000\arctan(1 - x)$. In this case, radiation passes through an optically thick medium near the left boundary and gets into the region with a gradually reducing optical opacity. In Fig. 8(a) we compare the solutions of the UGKWP method and the Monte Carlo method at $t = 1000$ and they agree with each

Table 1
Comparison of computational time of the Monte Carlo method and the UGKWP method for inflow into homogeneous medium under different parameters.

ϵ	MC	UGKWP
1	0.12s	0.14s
10^{-2}	1.49s	1.35s
10^{-4}	2587s	16s

Table 2
Comparison of the maximum number of particles used by the Monte Carlo method and the UGKWP method for inflow into homogeneous medium under different parameters.

ϵ	MC	UGKWP
1	13053	15612
10^{-2}	8054	6920
10^{-4}	8343	0

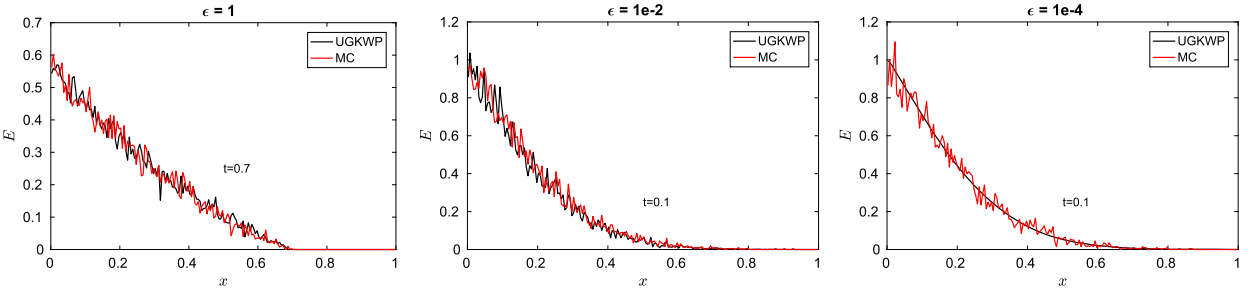

(a) Comparison of E between the UGKWP solution and the Monte Carlo solution for $\epsilon = 1$.

(b) Comparison of E between the UGKWP solution and the Monte Carlo solution for $\epsilon = 10^{-2}$.

(c) Comparison of E between the UGKWP solution and the Monte Carlo solution for $\epsilon = 10^{-4}$.

Fig. 7. Numerical results of homogeneous medium. (For interpretation of the colors in the figure(s), the reader is referred to the web version of this article.)

other closely. Also, in this case where the medium is relatively optically thick overall, the UGKWP produces much smoother solution than that given by the Monte Carlo method. For this test case, the Monte Carlo method uses a maximum of 17972 particles and takes 5127 seconds. The UGKWP method uses a maximum of 85 particles and takes 18 seconds. Therefore, the UGKWP method is much more efficient than the Monte Carlo method for this test case.

For the second test case, we use $\sigma = 100/\arcsin(1-x)$, where the medium gets more and more optically thick from the left to right boundaries. In Fig. 8(b) the numerical result of the UGKWP method is compared with the solution of the Monte Carlo method at $t = 20$ and they are almost identical except for the statistical noise. The Monte Carlo method uses a maximum of 24598 particles and spends 12 seconds while the UGKWP method uses a maximum of 24823 particles and spends 10 seconds in computing this case. In this test case the overall medium is relatively optically thin, and the UGKWP method has similar time cost as the Monte Carlo method.

6.3. Marshak wave problem

This section studies the Marshak wave problem where radiation is coupled with material medium. Consider the system

$$\begin{cases} \dfrac{1}{c}\dfrac{\partial I}{\partial t} + \mu \dfrac{\partial I}{\partial x} = \sigma\left(\dfrac{1}{2}acT^4 - I\right), \\ C_v \dfrac{\partial T}{\partial t} = \sigma\left(\displaystyle\int_{-1}^{1} I(\mu)\,\mathrm{d}\mu - acT^4\right) \end{cases}$$

for semi-infinite domain $x \in [0, +\infty)$ with a computational one $x \in [0, 0.5]$. The absorption coefficient is taken to be $\sigma = 30/T^3$, the speed of light $c = 29.98$, the parameter $a = 0.01372$ and the specific heat $C_v = 0.3$. The initial material temperature is set to be 10^{-2} and initially material and radiation energy are at equilibrium. A constant isotropic inflow

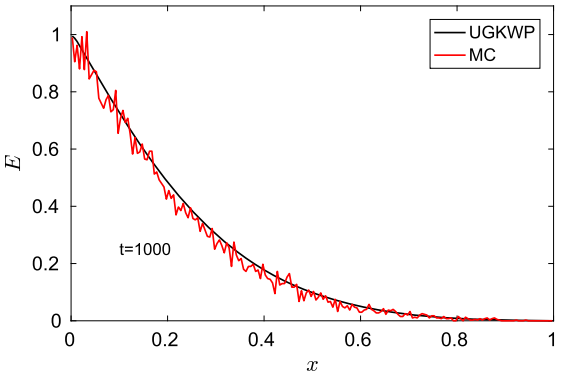

(a) Comparison of E between the UGKWP solution and the Monte Carlo solution in thick-to-thin heterogeneous medium.

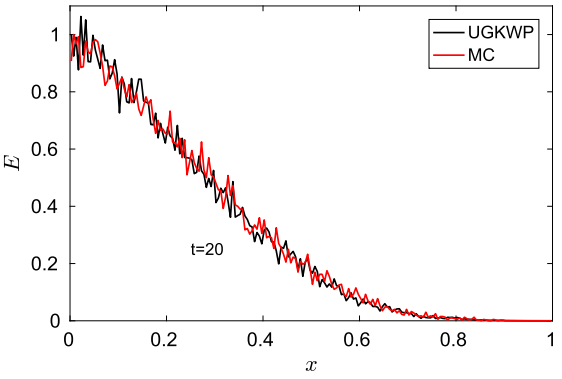

(b) Comparison of E between the UGKWP solution and the Monte Carlo solution in thin-to-thick heterogeneous medium.

Fig. 8. Numerical results of heterogeneous medium.

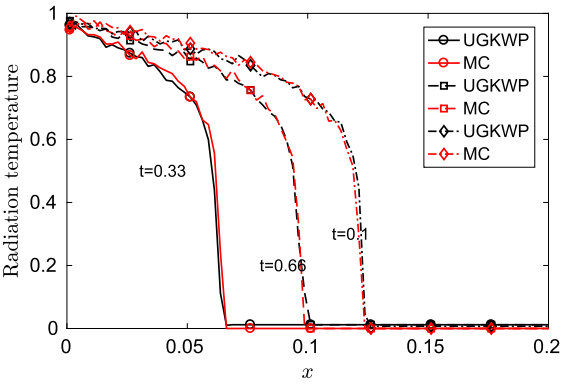

(a) Comparison of radiation temperature between the UGKWP solution and the Monte Carlo solution for Marshak wave problem.

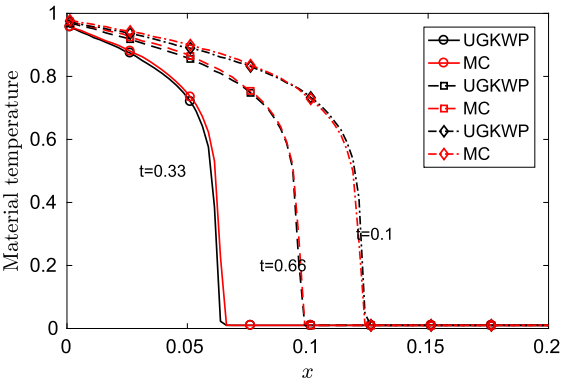

(b) Comparison of material temperature between the UGKWP solution and the Monte Carlo solution for Marshak wave problem.

Fig. 9. Numerical results of Marshak wave problem.

radiation intensity with an equivalent radiation temperature of 1 is imposed on the left boundary. Both the UGKWP method and the Monte Carlo method use 200 cells in space. For this example, the implicit Monte Carlo method uses a maximum of 45277 particles, while the UGKWP method uses a maximum of 42892 particles. It takes the implicit Monte Carlo method 66 seconds to compute until $t = 1.0$ and the UGKWP method uses 60 seconds.

In Fig. 9(a), the computed radiation wave front at time $t = 0.33$, 0.66 and 1.0 are given, while Fig. 9(b) presents the computed material temperature. The solutions of the UGKWP method are shown to be consistent with those of the Monte Carlo method for both radiation and material temperature.

6.4. Line-source problem in purely scattering homogeneous medium

The next problem is the line-source problem in purely scattering medium. In this test case, Eq. (3) is considered for $\epsilon = 1$, $\sigma = 1$ and $c = 1$. The spatial 2D computational domain is $[-1.5, 1.5] \times [-1.5, 1.5]$. The initial density distribution is

$$I(0, \mathbf{x}, \mathbf{\Omega}) = \frac{1}{4\pi}\delta(x)\delta(y),$$

which means that initially all particles are concentrated at $x = y = 0$ and they spread out over the time. This is a particularly difficult problem for the S_n based methods because they suffer from severe ray effect. Previous studies use this problem for comparison between different methods [38] and as a test case for schemes to mitigate the ray effect [39].

Both UGKWP method and the Monte Carlo method use 201×201 cells in space. The UGKWP method uses 1.633×10^7 particles while the Monte Carlo method uses 1.638×10^7 particles on the same spatial mesh. Because this example considers the kinetic regime, the number of particles used in the UGKWP method is almost the same as that used in the Monte Carlo

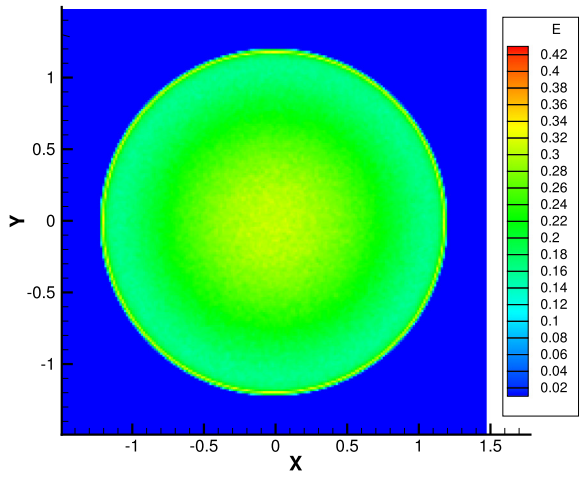

(a) Contour plot of the solution of E by the Monte Carlo method as a function of the spatial coordinate in the line-source problem at t = 1.2.

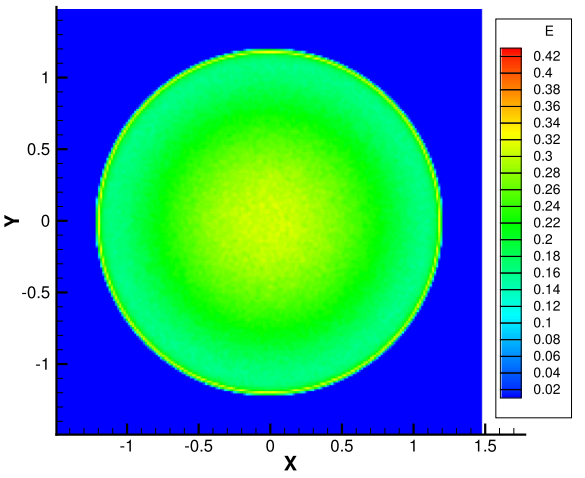

(b) Contour plot of the solution of E by the UGKWP method as a function of the spatial coordinate in the line-source problem at t = 1.2.

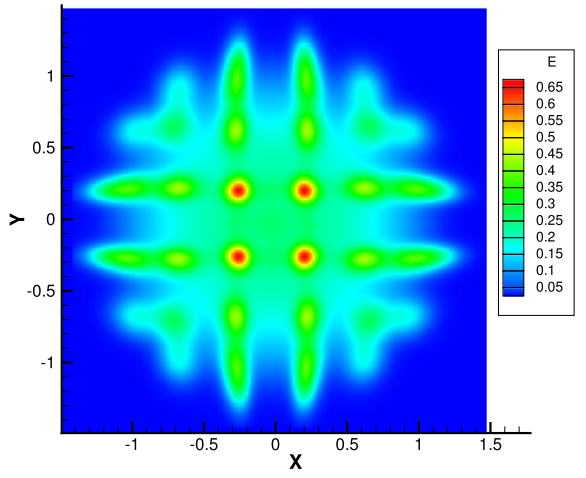

(c) Contour plot of the solution of E by the S_8 method as a function of the spatial coordinate in the line-source problem at t = 1.2.

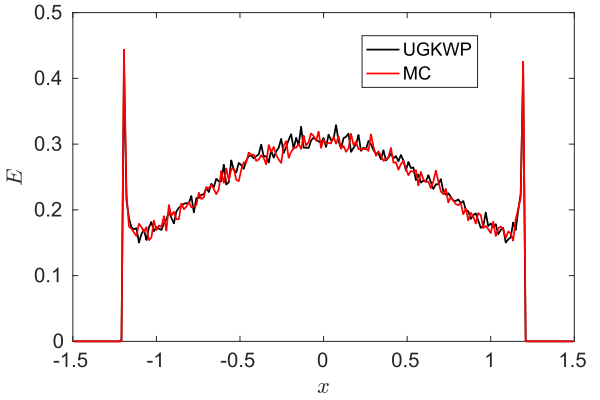

(d) Slice at y = 0 of the solution of E by the Monte Carlo method and the UGKWP method as a function of x in the line-source problem at t = 1.2.

Fig. 10. Numerical results of the line-source problem.

method and the computation time is 1530 seconds for the UGKWP method and 1034 seconds for the Monte Carlo method, where the UGKWP method is more expensive than Monte Carlo method in the highly rarefied regime due to its additional overheads.

Fig. 10 compares the solution of E between the UGKWP method, the Monte Carlo method and the S_8 method at time $t = 1.2$. For the S_8 computation, we use an equal-weight quadrature set, 201×201 cells for the spatial mesh and the DOM-UGKS. The UGKWP solution is consistent with the Monte Carlo solution. Both solutions display a sharp spike near the wave front and has a smooth nonzero region behind the wave front, and neither suffers from the ray effect. On the other hand, the S_8 solution is qualitatively incorrect due to the ray effect. This example demonstrates that the UGKWP method preserves the advantage of the Monte Carlo method in the rarefied regime without suffering from the ray effect.

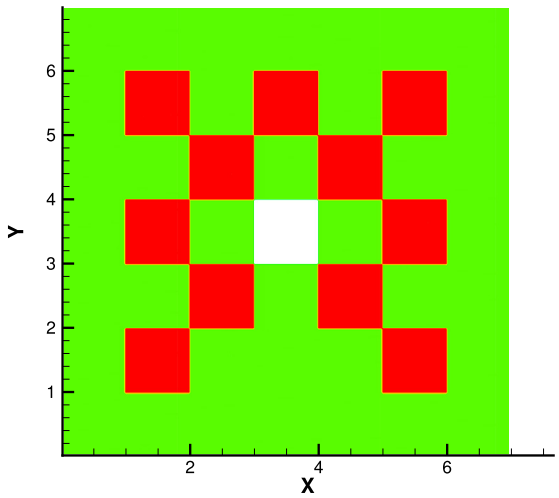

Fig. 11. Layout of the lattice problem.

6.5. Emitting isotropic source in lattice medium

In this section we study a problem with multiple medium [40] by considering the following equation

$$\begin{cases} \dfrac{\epsilon^2}{c}\dfrac{\partial I}{\partial t} + \epsilon \boldsymbol{\Omega}\cdot\nabla I = \sigma_a\left(\dfrac{1}{4\pi}acT^4 - I\right) + \sigma_s\left(\dfrac{1}{4\pi}E - I\right) + \epsilon^2 G, \\ \epsilon^2 C_v \dfrac{\partial T}{\partial t} = b\Delta T + \sigma_a\left(\displaystyle\int_{\mathbb{S}^2} I(\boldsymbol{\Omega})\,\mathrm{d}\boldsymbol{\Omega} - acT^4\right). \end{cases}$$

The diffusion term $b\Delta T$ is solved by using a backward Euler method. The two-dimensional physical space $[0,7]\times[0,7]$ consists of a set of squares belonging to a strongly absorbing medium and a background of weakly scattering medium. The specific layout of the problem is given in Fig. 11, where the light green regions and the white region are purely scattering medium with $\sigma_s = 2$ and $\sigma_a = 0$; the red regions contain purely absorbing material with $\sigma_s = 0$ and $\sigma_a = 2000$. In the white region at the center there is an isotropic source $G = \dfrac{1}{4\pi}$. The initial material temperature is 10^{-2} and initially the radiation and material temperature are at equilibrium. In simulating the case, the parameters are taken as $C_v = 0.3$, $b = 0.03$ and $c = a = \epsilon = 1$. Both the UGKWP method and the Monte Carlo method use a mesh of 280×280 in physical space. The results at time $t = 2$ are summarized in Fig. 12 with the natural logarithm of density distribution shown in contour and slice, and they are in agreement with each other. This is a test case with both kinetic and diffusive regimes. Most of the time particles travel in the kinetic regime. The Monte Carlo method uses 10^8 particles and took 5692 seconds, while the UGKWP method uses 8.5×10^7 particles and took 3092 seconds, showing the UGKWP method to be more efficient than the Monte Carlo method for this case where there is mixed medium.

6.6. A hohlraum problem

This example considers a hohlraum problem similar to the one studied in [40]. We study equation (38) with $G = 0$. The problem layout is given in Fig. 13. This is a problem of purely absorbing medium where the absorption coefficient relies on the material temperature. As the material temperature varies, the values of the absorption coefficient cover a wide range values, presenting challenges to numerical methods. On the left boundary there is an isotropic source with the specific intensity $I(\boldsymbol{\Omega}) = \dfrac{1}{4\pi}$. Initially radiation and material temperature are at equilibrium and the initial material temperature is $T = 10^{-2}$.

The UGKWP method uses 400×400 cells in space while the Monte Carlo method use 800×800 cells in space. The output time is $t = 2$. The Monte Carlo method uses a maximum of 2×10^7 particles and takes 9.8 hours. The UGKWP method uses a maximum of 3×10^6 particles and takes 1406 seconds, therefore the UGKWP method is 25 times more efficient than the Monte Carlo method for this test case. For this test, the initial absorption coefficient on the boundary is extremely large, and the Monte Carlo method takes an especially long time in the first time steps when the inflow radiation heats up the boundary material. The UGKWP method, on the other hand, has no such problem.

This test should contain two characteristic solutions [40]. The central block should be heated non-uniformly; and the region to the right of the block, which is not within the line of sight of the source, should have lower radiation energy

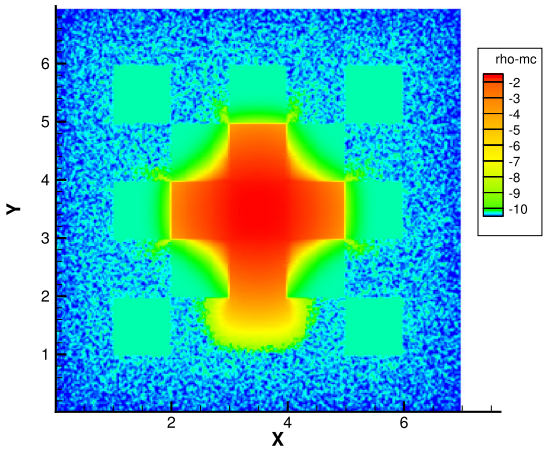

(a) Contour plot of the solution of $\ln E$ by the Monte Carlo method as a function of the spatial coordinate in the lattice problem at $t = 2$.

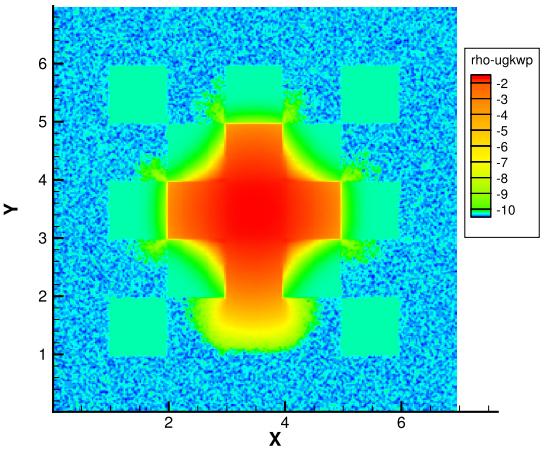

(b) Contour plot of the solution of $\ln E$ by the UGKWP method as a function of the spatial coordinate in the lattice problem at $t = 2$.

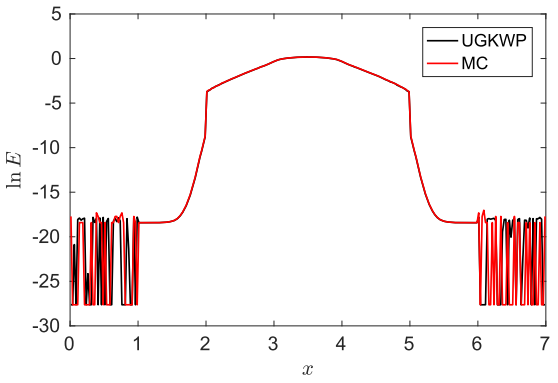

(c) Slice at $y = 0$ of the solution of $\ln E$ by the Monte Carlo method and UGKWP as a function of x in the lattice problem at $t = 2$.

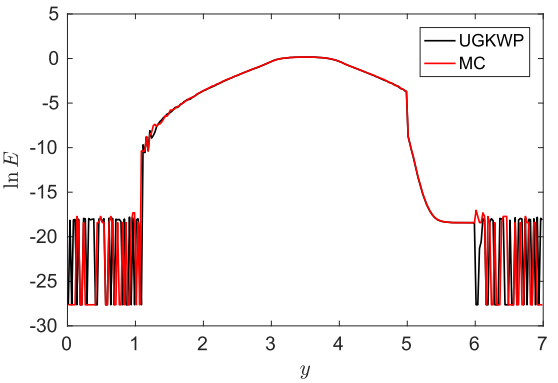

(d) Slice at $x = 0$ of the solution of $\ln E$ by the Monte Carlo method and UGKWP as a function of y in the lattice problem at $t = 2$.

Fig. 12. Numerical results of the lattice problem.

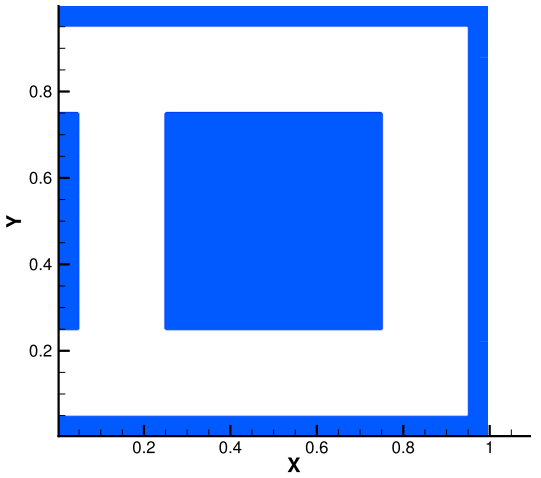

Fig. 13. Layout of the hohlraum problem. In the blue regions $\sigma_a = 1000T^{-3}$, $\sigma_s = 0$ and $C_v = 0.3$. The white region is vacuum, $\sigma_a = \sigma_s = 0$.

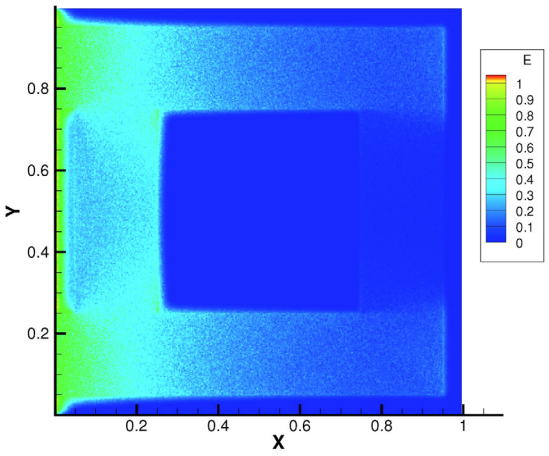

(a) Contour plot of the solution of E by the Monte Carlo method as a function of the spatial coordinate in the hohlraum problem at $t = 2$.

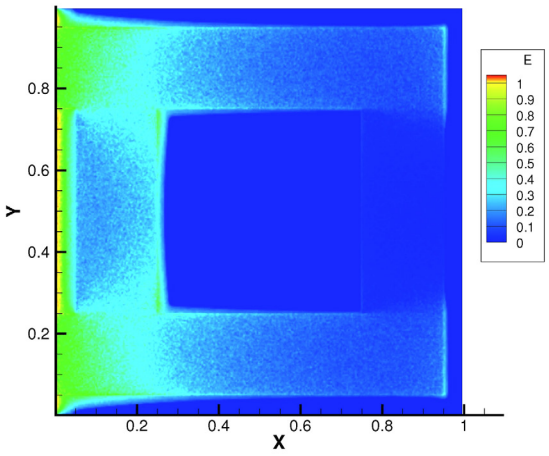

(b) Contour plot of the solution of E by the UGKWP method as a function of the spatial coordinate in the hohlraum problem with at $t = 2$.

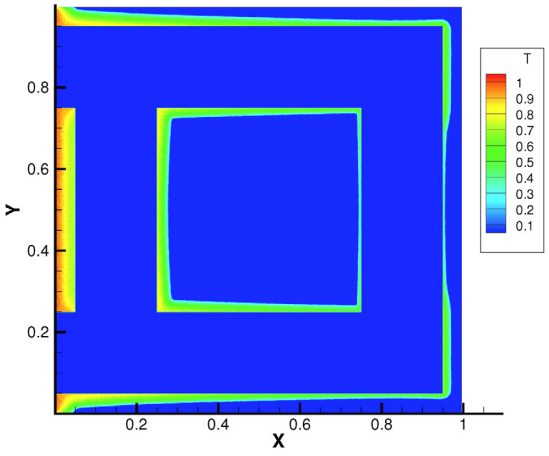

(c) Contour plot of the solution of T by the Monte Carlo method as a function of the spatial coordinate in the hohlraum problem at $t = 2$.

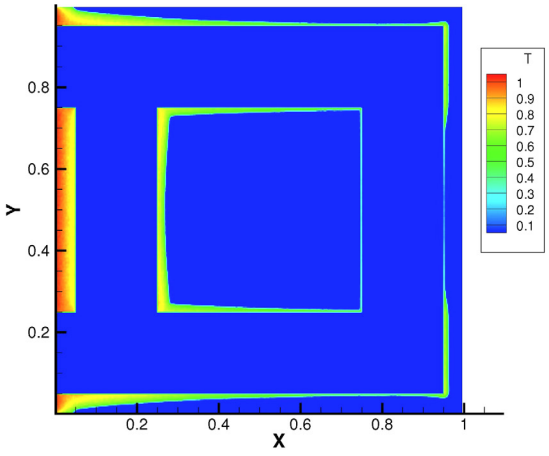

(d) Contour plot of the solution of T by the UGKWP method as a function of the spatial coordinate in the hohlraum problem with at $t = 2$.

Fig. 14. Numerical results of the hohlraum problem I.

than that in regions which could be directly radiated by the source. The previous studies in [40] showed that the diffusion equation could not capture these two characteristics. In Fig. 14 and 15, we compare the solution of the UGKWP method and the Monte Carlo method for energy density and material temperature at $t = 2$ and they are all consistent with each other. Both solutions agree with each other very well. There is less radiation behind the block with respect to the source. This test shows that the UGKWP method keeps the accuracy as the Monte Carlo method and becomes more accurate than the diffusion approximation in problem which has essentially a multiscale nature.

7. Conclusion

In this paper, for the first time a unified gas-kinetic wave-particle method is proposed to simulate photon transport. Due to the particle-wave decomposition and their dynamic coupling, the UGKWP method becomes a multiscale method to simulate transport process with the adoption of the most efficient way in different regimes. For the linear transport equation, this method recovers the solution of the diffusion equation in the optically thick limit without constraint on the time step being less than the photon's mean collision time. At the same time, it gives the exact solution in the free transport

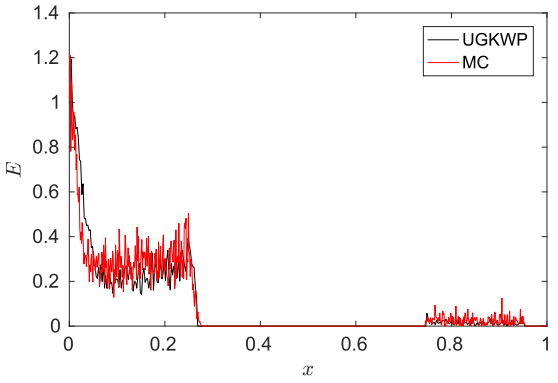

(a) Comparison of sliced solution at $y = 0$ of the solution of E by the UGKWP method and the Monte Carlo method as a function of x coordinate in the hohlraum problem at $t = 2$.

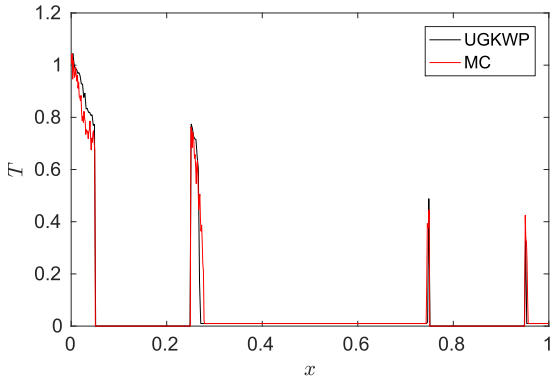

(b) Comparison of sliced solution at $y = 0$ of the solution of T by the UGKWP method and the Monte Carlo method as a function of x coordinate in the hohlraum problem at $t = 2$.

Fig. 15. Numerical results of the hohlraum problem II.

regime. In the transition regime, both macroscopic wave and kinetic particle contribute to the radiative transfer, and their weights and coupling depend on the ratio of the time step to the local particle's mean collision time. The UGKWP method is also extended to the coupled radiation-material system. With the inclusion of energy exchange, the UGKWP method can give excellent simulation results in different regimes. A few benchmark problems are tested to show the performance of the current scheme. The accuracy and efficiency of the UGKWP method are fully confirmed. For the multiscale transport with the co-existence of different regimes, the UGKWP method may improve the efficiency on several-order-of-magnitude in comparison with the purely particle method. The UGKWP method takes also advantages of both particle and macroscopic solver. The UGKWP method has totally removed the ray effect and has a much improved efficiency in comparison with DOM-type UGKS in rarefied regime. Based on the direct modeling of the transport physics in the time step scale [30], such as the relationship between t_f and Δt in the current study, we have three versions of UGKS for the multiscale transport simulations, i.e., the DOM or DVM-type UGKS, the purely particle UGKP, and the wave-particle UGKWP. Under different flow conditions, there are advantages and disadvantages among these different discretization under the same UGKS multiscale modeling. The extension of these schemes to complex systems, such as radiative-hydrodynamics, plasma, multi-component system, and reactive flow, will be further investigated.

Declaration of competing interest

The authors declare that they have no known conflict of interest in this paper.

Acknowledgement

The current research is supported by Hong Kong research grant council (16206617), and National Science Foundation of China (11472219, 11772281, 11701038, 91852114, 11771035, U1530401).

References

[1] S.W. Davis, J.M. Stone, Y.-F. Jiang, A radiation transfer solver for Athena using short characteristics, Astrophys. J. Suppl. Ser. 199 (1) (2012) 9.
[2] A. Marshak, A. Davis, 3D Radiative Transfer in Cloudy Atmospheres, Springer Science & Business Media, 2005.
[3] A.D. Klose, U. Netz, J. Beuthan, A.H. Hielscher, Optical tomography using the time-independent equation of radiative transfer, part 1: forward model, J. Quant. Spectrosc. Radiat. Transf. 72 (5) (2002) 691–713.
[4] B. Hunter, Z. Guo, Comparison of quadrature schemes in DOM for anisotropic scattering radiative transfer analysis, Numer. Heat Transf., Part B, Fundam. 63 (6) (2013) 485–507.
[5] P.J. Coelho, Advances in the discrete ordinates and finite volume methods for the solution of radiative heat transfer problems in participating media, J. Quant. Spectrosc. Radiat. Transf. 145 (2014) 121–146.
[6] S.-S. Chen, B.-W. Li, Y.-S. Sun, Chebyshev collocation spectral method for solving radiative transfer with the modified discrete ordinates formulations, Int. J. Heat Mass Transf. 88 (2015) 388–397.
[7] T. Roos, T. Harms, C. du Toit, Conservation of scattered energy and asymmetry factor in the new rotationally symmetric spherical discretisation scheme, Int. J. Heat Mass Transf. 101 (2016) 205–225.
[8] M. Frank, B. Dubroca, A. Klar, Partial moment entropy approximation to radiative heat transfer, J. Comput. Phys. 218 (1) (2006) 1–18.
[9] J.A. Carrillo, T. Goudon, P. Lafitte, F. Vecil, Numerical schemes of diffusion asymptotics and moment closures for kinetic equations, J. Sci. Comput. 36 (1) (2008) 113–149.
[10] V. Vikas, C. Hauck, Z. Wang, R.O. Fox, Radiation transport modeling using extended quadrature method of moments, J. Comput. Phys. 246 (2013) 221–241.

[11] G.W. Alldredge, R. Li, W. Li, Approximating the M_2 method by the extended quadrature method of moments for radiative transfer in slab geometry, Kinet. Relat. Models 9 (2) (2016) 237–249.
[12] J. Fleck, J. Cummings, An implicit Monte Carlo scheme for calculating time and frequency dependent nonlinear radiation transport, J. Comput. Phys. 8 (3) (1971) 313–342.
[13] L. Lucy, Computing radiative equilibria with Monte Carlo techniques, Astron. Astrophys. 344 (1999) 282–288.
[14] C.K. Hayakawa, J. Spanier, V. Venugopalan, Coupled forward-adjoint Monte Carlo simulations of radiative transport for the study of optical probe design in heterogeneous tissues, SIAM J. Appl. Math. 68 (1) (2007) 253–270.
[15] J. Fleck Jr, E. Canfield, A random walk procedure for improving the computational efficiency of the implicit Monte Carlo method for nonlinear radiation transport, J. Comput. Phys. 54 (3) (1984) 508–523.
[16] J. Giorla, R. Sentis, A random walk method for solving radiative transfer equations, J. Comput. Phys. 70 (1) (1987) 145–165.
[17] J.D. Densmore, T.J. Urbatsch, T.M. Evans, M.W. Buksas, A hybrid transport-diffusion method for Monte Carlo radiative-transfer simulations, J. Comput. Phys. 222 (2) (2007) 485–503.
[18] J.D. Densmore, K.G. Thompson, T.J. Urbatsch, A hybrid transport-diffusion Monte Carlo method for frequency-dependent radiative-transfer simulations, J. Comput. Phys. 231 (20) (2012) 6924–6934.
[19] A. Klar, An asymptotic-induced scheme for nonstationary transport equations in the diffusive limit, SIAM J. Numer. Anal. 35 (3) (1998) 1073–1094.
[20] G. Naldi, L. Pareschi, Numerical schemes for kinetic equations in diffusive regimes, Appl. Math. Lett. 11 (2) (1998) 29–35.
[21] S. Jin, Efficient asymptotic-preserving (AP) schemes for some multiscale kinetic equations, SIAM J. Sci. Comput. 21 (2) (1999) 441–454.
[22] S. Jin, L. Pareschi, G. Toscani, Uniformly accurate diffusive relaxation schemes for multiscale transport equations, SIAM J. Numer. Anal. 38 (3) (2000) 913–936.
[23] L. Mieussens, On the asymptotic preserving property of the unified gas kinetic scheme for the diffusion limit of linear kinetic models, J. Comput. Phys. 253 (2013) 138–156.
[24] W. Sun, S. Jiang, K. Xu, An asymptotic preserving unified gas kinetic scheme for gray radiative transfer equations, J. Comput. Phys. 285 (2015) 265–279.
[25] W. Sun, S. Jiang, K. Xu, S. Li, An asymptotic preserving unified gas kinetic scheme for frequency-dependent radiative transfer equations, J. Comput. Phys. 302 (2015) 222–238.
[26] W. Sun, S. Jiang, K. Xu, A multidimensional unified gas-kinetic scheme for radiative transfer equations on unstructured mesh, J. Comput. Phys. 351 (2017) 455–472.
[27] W. Sun, S. Jiang, K. Xu, An implicit unified gas kinetic scheme for radiative transfer with equilibrium and non-equilibrium diffusive limits, Commun. Comput. Phys. 22 (4) (2017) 889–912.
[28] W. Sun, S. Jiang, K. Xu, An asymptotic preserving implicit unified gas kinetic scheme for frequency-dependent radiative transfer equations, Int. J. Numer. Anal. Model. 15 (1–2) (2018) 134–153.
[29] K. Xu, J.-C. Huang, A unified gas-kinetic scheme for continuum and rarefied flows, J. Comput. Phys. 229 (20) (2010) 7747–7764.
[30] K. Xu, Direct Modeling for Computational Fluid Dynamics: Construction and Application of Unified Gas-Kinetic Schemes, World Scientific, 2015.
[31] D. Jiang, M. Mao, J. Li, X. Deng, An implicit parallel UGKS solver for flows covering various regimes, Adv. Aerodyn. 1 (2019), https://doi.org/10.1186/s42774--019--0008--5.
[32] C. Liu, K. Xu, A unified gas kinetic scheme for continuum and rarefied flows V: multiscale and multi-component plasma transport, Commun. Comput. Phys. 22 (5) (2017) 1175–1223.
[33] C. Liu, Z. Wang, K. Xu, A unified gas-kinetic scheme for continuum and rarefied flows VI: dilute disperse gas-particle multiphase system, J. Comput. Phys. 386 (2019) 264–295.
[34] K. Xu, C. Liu, A paradigm for modeling and computation of gas dynamics, Physics of Fluids 29, 026101.
[35] C. Liu, Y. Zhu, K. Xu, Unified gas-kinetic wave-particle methods, I: continuum and rarefied gas flow, J. Comput. Phys. 401 (2020) 108977.
[36] Y. Zhu, C. Liu, C. Zhong, K. Xu, Unified gas-kinetic wave-particle methods, II: multiscale simulation on unstructured mesh, Phys. Fluids 31 (6) (2019) 067105.
[37] S. Jin, L. Pareschi, G. Toscani, Diffusive relaxation schemes for multiscale discrete-velocity kinetic equations, SIAM J. Numer. Anal. 35 (6) (1998) 2405–2439.
[38] T.A. Brunner, Forms of approximate radiation transport, Sandia National Laboratory, SAND2002-1778.
[39] T. Camminady, M. Frank, K. Küpper, J. Kusch, Ray effect mitigation for the discrete ordinates method through quadrature rotation, J. Comput. Phys. 382 (2019) 105–123.
[40] R.G. McClarren, C.D. Hauck, Robust and accurate filtered spherical harmonics expansions for radiative transfer, J. Comput. Phys. 229 (16) (2010) 5597–5614.